

Lawrence Berkeley National Laboratory

Recent Work

Title

SOME TECHNIQUES FOR STOCHASTIC MODELING OF THREE-DIMENSIONAL FRACTURE NETWORKS

Permalink

<https://escholarship.org/uc/item/6q88530z>

Authors

Hestir, K.
Long, J.
Chiles, J.P.

Publication Date

1988-02-01



Lawrence Berkeley Laboratory

UNIVERSITY OF CALIFORNIA

EARTH SCIENCES DIVISION

Presented at the DOE/AECL 87 Conference on Geostatistical, Sensitivity, and Uncertainty Methods for Ground-Water Flow and Radionuclide Transport Modeling, San Francisco, CA, September 15-17, 1988, and to be published in the Proceedings

RECEIVED
LAWRENCE
BERKELEY LABORATORY

APR 26 1988

LIBRARY AND
DOCUMENTS SECTION

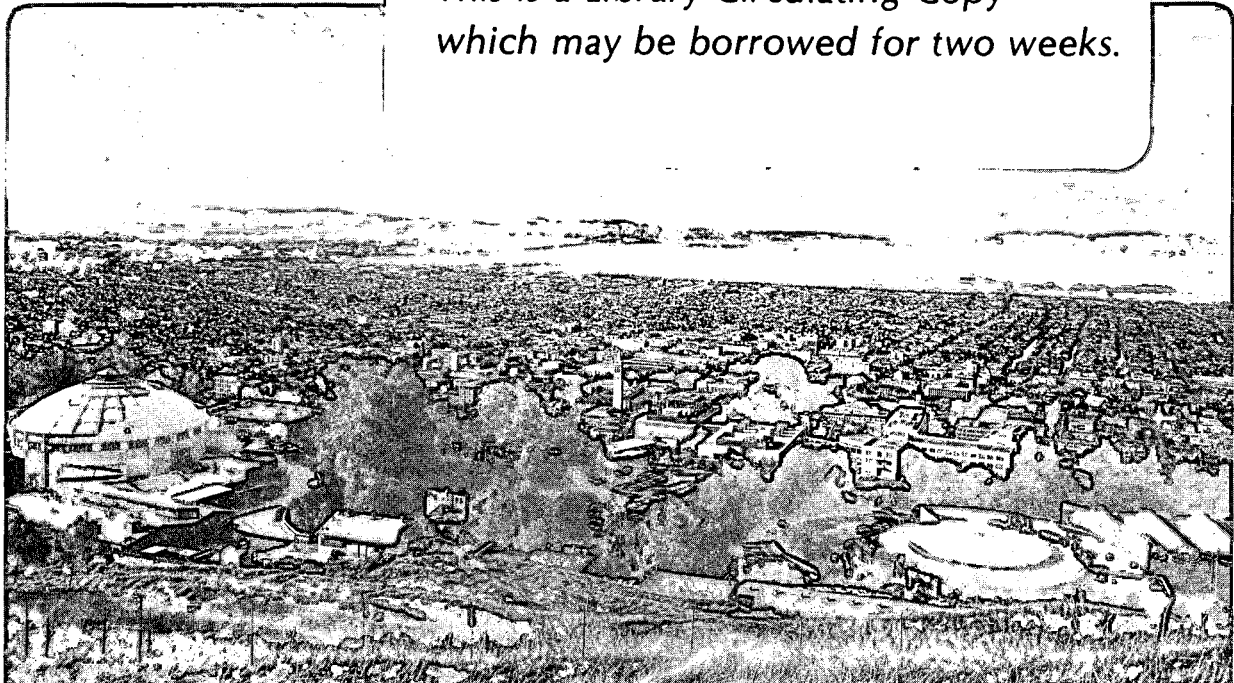
Some Techniques for Stochastic Modeling of Three-Dimensional Fracture Networks

K. Hestir, J. Long, J.-P. Chilès, and D. Billaux

February 1988

TWO-WEEK LOAN COPY

This is a Library Circulating Copy which may be borrowed for two weeks.



LBL-25826

DISCLAIMER

This document was prepared as an account of work sponsored by the United States Government. While this document is believed to contain correct information, neither the United States Government nor any agency thereof, nor the Regents of the University of California, nor any of their employees, makes any warranty, express or implied, or assumes any legal responsibility for the accuracy, completeness, or usefulness of any information, apparatus, product, or process disclosed, or represents that its use would not infringe privately owned rights. Reference herein to any specific commercial product, process, or service by its trade name, trademark, manufacturer, or otherwise, does not necessarily constitute or imply its endorsement, recommendation, or favoring by the United States Government or any agency thereof, or the Regents of the University of California. The views and opinions of authors expressed herein do not necessarily state or reflect those of the United States Government or any agency thereof or the Regents of the University of California.

**Some Techniques for Stochastic Modeling
of Three-Dimensional Fracture Networks**

Kevin Hestir and Jane Long

**Earth Sciences Division
Lawrence Berkeley Laboratory
1 Cyclotron Road
Berkeley, California 94720**

Jean-Paul Chilès

**Bureau de Recherches
Géologiques et Minières (BRGM)
Orléans, France**

Daniel Billaux

**Earth Sciences Division
Lawrence Berkeley Laboratory
1 Cyclotron Road
Berkeley, California 94720
On leave from BRGM**

Some Techniques for Stochastic Modeling of Three-Dimensional Fracture Networks

KEVIN HESTIR and JANE LONG
Earth Sciences Division
Lawrence Berkeley Laboratory
Berkeley, California

JEAN-PAUL CHILES
Bureau de Recherches
Géologiques et Minières (BRGM)
Orléans, France

DANIEL BILLAUX
Earth Sciences Division
Lawrence Berkeley Laboratory
Berkeley, California
on leave from BRGM

Abstract

This paper describes some new techniques for stochastic modeling of three-dimensional fracture networks. We use geostatistical simulation methods to reproduce features of the spatial structure of the rock such as the variation of fracture density and fracture orientation in space. For an example of the method we use mapped fracture data from the Fanay-Augeres mine, in Limousin, France. Two different sections of a drift wall, S1 and S2, were mapped. The S1 section is wet, and the S2 section is dry. For each case, the fractures are divided into five different sets and each set is modeled separately. The fractures in each set are represented as discs placed randomly in space. The diameter of each disc is chosen independently from a fixed probability distribution determined from the trace length distribution. For the location of discs a point process called the parent-daughter process is used. This process gives a clumping or swarming of fractures not found in the usual Poisson model. The orientation of the discs is characterized as a fluctuation about the mean orientation for the set. This fluctuation has a spatial structure that is simulated with geostatistics. Geostatistical simulations of the two fracture systems are under way. The connectivities of the simulations will be assessed to see if there is any correlation with the fact that the S1 section of drift is wet and the S2 section is dry.

Introduction

Over the past few years, attempts have been made to model the hydrology of fractured rock by collecting data on the individual fractures and synthesizing a model

of the hydraulically active fracture network. Numerical models that have been developed for this purpose include our own (Long et al., 1982; Long and Witherspoon, 1985) as well as those of Robinson (1984), Dershowitz (1984), Rouleau (1984), Cacas et al. (1987), and others. These models have in some cases been applied to the analysis of field data, for example Rouleau (1984), Cacas et al. (1987), and Long and Billaux (1987). In Long and Billaux, we explored some techniques for using geostatistics to model some of the spatial structures commonly observed in fracture systems. In particular, we modeled the spatial variation of fracture density in a two-dimensional case.

In this paper, we extend the techniques to the case of three-dimensional fractures where we can also simulate the variation of fracture density, and fracture orientation in space. Data on the conductivity of individual fractures are extremely difficult to obtain, and we did not have such data. Therefore we do not attempt to stochastically generate this parameter. As data on the conductivity of individual fractures are so rare, perhaps the best way to assign this parameter in the model is to use a backfitting method such as that employed by Cacas et al. (1987). We do not pursue this procedure in this work. Instead, we concentrate on defining the network geometry in space and examining its connectivity.

One of the major problems in stochastic fracture modeling is the inability to obtain appropriate data directly. An ideal situation for fracture network simulation would be to have three-dimensional data for some large piece of the network. These data would give the geometry and conductivity of each fracture, including any channeling that may occur within the fractures. With this hypothetical information we could generate simulations that would approximately match the three-dimensional flow system. That is, if we knew all the geometry, we could model the flow.

This sort of ideal fracture data is not available. Lack of three-dimensional data makes the problem we face in constructing a simulation much harder. Typically the data we have from fractured rock provide a one-dimensional view through a three-dimensional system, i.e., a borehole. At best, we may have a two-dimensional sample such as a drift wall mapping.

With "perfect" two-dimensional data we would perhaps have a solvable problem. In this case we would still need to determine the three-dimensional shape of the fractures and the nature of flow through those fractures. Unfortunately, even interpreting correct statistics from two-dimensional data is difficult due to biases in sampling techniques.

The lack of three-dimensional data compounded with the less than "perfect" nature of two-dimensional data creates the requirement that we make some reasonable assumptions about the three-dimensional structure of the fracture network. These assumptions are used to build our conceptual model for the fracture mesh. The simulation is then based on the conceptual model.

The conceptual model we use here represents fractures as thin discs in three-dimensional space. The location of a disc is defined as the location of its center. The placement of fracture centers is determined by a stochastic process called the parent-daughter point process which is described below. Diameters of discs are assumed to be independent random variables. Orientation of fractures is taken to be a stationary random field. We will base the parameters of this model on the analysis of drift wall mapping data collected at the uranium mine of Fanay-Augères, in Limousin, France.

This paper gives the details of the conceptual model and the construction of these simulations. In a future paper, we will present the actual numerical simulations of fracture networks and an examination of the connectivity of these simulations.

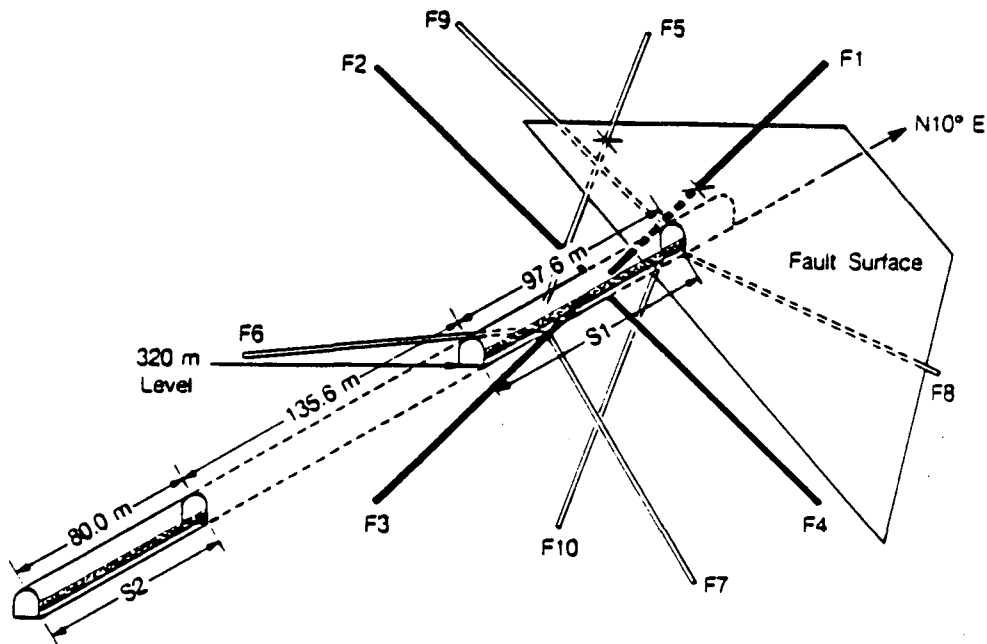
Our presentation is divided into the following parts:

1. A description of the data.
2. Description of a conceptual model for the system.
3. Use of the data to determine the parameters required by the conceptual model.
4. Description of the techniques for numerical simulation of the fracture systems.
5. Conclusions.

Fanay-Augères Data

Fanay-Augères is a uranium mine owned by Cogema Co. and located in Limousin, France in the granite massif of Saint-Sylvestre. Since 1980 this mine has been used as a test facility to develop methods and tools for investigating mass and heat transfer in granitic rocks (Barbreau et al., 1985; Lassagne, 1983).

We focus on the data collected in a long section of a drift, about 3 m in diameter at the 320-m level (Figure 1). In this drift fractures on the east wall have



XBL 884-10184

Figure 1. Perspective view of experimental gallery and boreholes.

been mapped over two sections, S1 and S2, totaling 180 m in length. S1 is 100 m in length and S2 is 80 m. We construct two simulations, one using data from S1 and one using data from S2. For any fracture trace which intersected a 2-m-high rectangle, the visible trace length, number and location of visible endpoints, orientation, and morphology were recorded. For 80% of the mapped fractures both endpoints were visible.

Ten boreholes 50 m long were drilled in three radial patterns (Figure 1). Oriented core was obtained from these holes and the fractures logged. More than 220 steady-state permeability tests were performed in these holes between packers spaced at various distances. In summary, these data provided information about the location, size, and characteristics of about 7000 fractures.

A usual step in fracture analysis is to divide fractures into sets and model each set separately. We have followed this course as explained in Long and Billau (1987). Gros (1982) gives an analysis of the fracturing at Fanay-Augères that identifies seven major tectonic episodes from which he defined five major sets of fractures by their orientation. However, 60% of the fractures do not fall into any of the tectonic classes. This classification is clearly not adequate for our purposes. Therefore, we have broadened the definition of the sets so that 98% of the fractures mapped in S1 (1059 out of 1076) and 95% of the fractures mapped in S2 (1115 out of 1177) are included. The resulting classification, based on orientation, is illustrated with a lower hemisphere equal area stereonet in Figure 2. Figure 3 shows the fracture traces from S1 and S2.

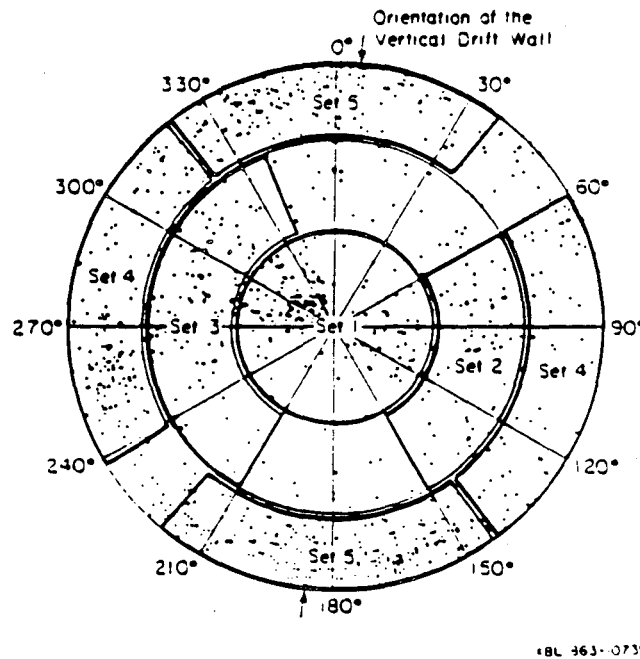


Figure 2. Lower hemisphere Schmidt stereonet of fracture poles showing set boundaries.

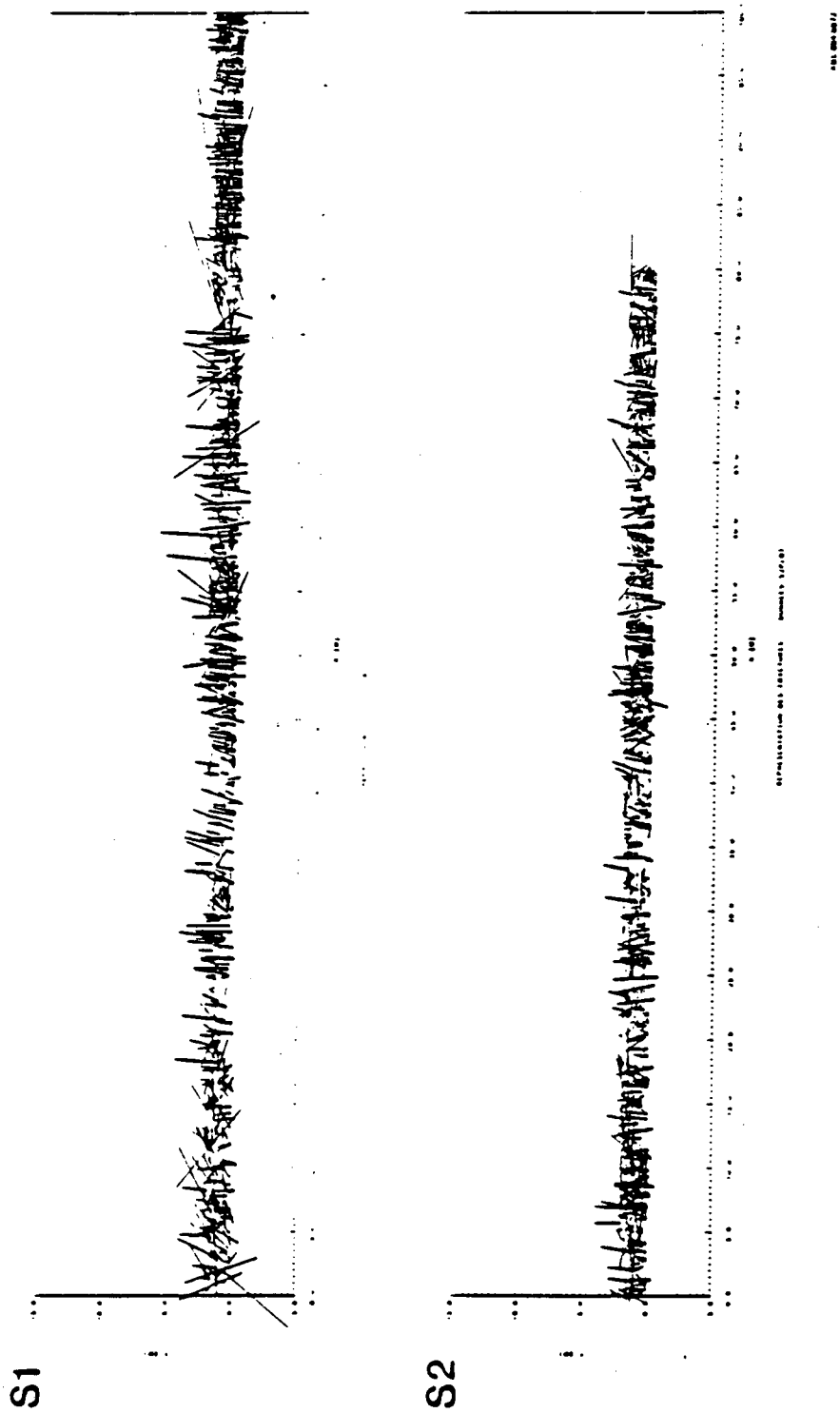


Figure 3. Traces of fractures from sections S1 and S2.

In summary, there are two data sets, one for S1 and one for S2. Each data set consists of the location and truncation of trace endpoints, and for each trace, an orientation and set classification.

Description of the Conceptual Model

The choice of a stochastic conceptual model for a three-dimensional fracture system involves specifying:

1. Individual characteristics of the fractures such as shape, size, orientation, aperture, or transmissivity.
2. The arrangement of the fractures in space, defined by the type of point process their locations follow and the way they truncate each other.

When dealing with three-dimensional fracture systems, many of these choices must be made somewhat arbitrarily because we can only take one-dimensional or two-dimensional samples from the three-dimensional system. However, once these choices are made, we can derive some of the statistical relationships between the parameters of the three-dimensional model we have chosen and the statistics that can be measured in the field. Except in the simple Poisson case, these statistical relationships do not give us a direct estimate of the parameters of the three-dimensional model, but rather enable us to derive the statistical properties on the plane from a guess at these parameters. So by trial and error we can match the observed statistics. We typically find that there are many different choices for parameters of the three-dimensional model that give the same two-dimensional statistics. We will call each of these choices a *parameter solution*. Hence, in statistical terminology, our problem is ill-posed, i.e., the data do not determine a unique parameter solution.

Individual characteristics of the fractures

We model fractures as circular discs in space. The disc assumption is reasonable in the absence of evidence on the actual shape of fractures, because it is the simplest possible assumption.

The distribution of disc diameters is assumed to be lognormal, independent of all other quantities in the model. Using this assumption it is possible to fit the field distribution of trace lengths with the distribution derived from lognormal distribution of diameters. Here we find a simple example of the limitations of two-dimensional data. One can show that large changes in the diameter distribution will result in small changes in the trace length distribution. Hence, any small change in the trace length distribution will have a large effect on the estimated diameter distribution. This illustrates the ill-posed character of our problem. A nice summary of the problem of estimating diameter distributions from trace lengths is given in the introduction in O'Sullivan (1986).

Orientation is assumed to be a stationary random function independent of all other quantities in the model. Because we have a different model for each set and fractures within a set have similar orientations, the probability model for orientation is a relatively simple one and other parameters are automatically correlated with orientation. On the other hand, it is difficult to find spatial relationships between fractures of different sets with this model.

Point processes and placement of fractures

Our approach to choosing a point process for locating fracture centers is to examine semivariograms of the three-dimensional point processes projected onto the two-dimensional plane. We will call these variograms the *trace density semivariograms*. We choose the theoretical three-dimensional point process that has a trace density semivariogram closest to the trace density semivariogram from the data. This analysis is discussed below.

A point process is defined as a random phenomenon, each realization of which is a set of various points dispersed in space, with no infinite accumulation in any bounded subset. The two-dimensional sample we work with is a realization of fracture traces as shown in Figure 3 for S1 and S2. Placing points at the centers of traces creates the two-dimensional point process which is the projection of the original three-dimensional process we wish to determine.

For any point process N , we define the random variable $N(B)$ as the number of points inside a set B . To examine the structure of point processes in two dimensions we use the following definitions. Let \bar{x} denote a point in two-space, R^2 . $B_{\bar{x}}$ will denote a small subset of R^2 , for example a square, centered on the point \bar{x} . N will denote a point process which is a two-dimensional projection of a three-dimensional point process. We define the semivariogram, $\gamma(\bar{x}, \bar{y})$, of $N(B_{\bar{x}})$ via

$$\gamma(\bar{x}, \bar{y}) = \frac{1}{2} E((N(B_{\bar{x}}) - N(B_{\bar{y}}))^2).$$

For the point processes we consider, $\gamma(\bar{x}, \bar{y})$ is a function of only the difference, $\bar{x} - \bar{y}$. This is the standard property of second-order stationarity. For a discussion of the geostatistical terminology concerning semivariograms see, for example, Journel and Huijbregts (1978). This terminology is used freely in the following.

Below, several candidate point processes and their trace density semivariograms are described. For a general overview of point processes the interested reader should consult Ripley (1981) or Stoyan et al. (1987).

The Poisson process

The simplest and most widely used point process for placement of fractures is the Poisson process. The projection of a Poisson process into two-dimensional space is again a Poisson process. If a point process N is Poisson with density λ , then $N(B)$ is a Poisson random variable with rate λA where $A = \text{area}(B)$. This implies that $E(N(B_{\bar{x}})) = \text{Var}(N(B_{\bar{x}}))$. Also for a Poisson process, $N(B_1)$ and $N(B_2)$ are independent random variables when B_1 and B_2 are disjoint. This implies the semivariogram of $N(B_{\bar{x}})$ is a pure nugget when $|\bar{x} - \bar{y}|$ is large enough so that $B_{\bar{x}}$ and $B_{\bar{y}}$ are disjoint.

The regionalized Poisson process

This is a Poisson process with a density varying in space. The density is a stationary random function, which, if Gaussian, can be characterized by its semivariogram and constant mean. In this case the semivariogram of $N(B_{\bar{x}})$ now has a structure, but locally, when the random density has a small variance, $N(B_{\bar{x}})$ is

approximately equal to its mean as in the pure Poisson process. Such point processes are also known as doubly stochastic Poisson processes. Doubly stochastic processes are very general and theoretically include the parent-daughter processes. However, in our case the density can have a large variance and is best characterized using the processes described below.

The parent-daughter process

Starting from a Poisson process, a cloud of points (or daughters) is placed around each point (called a parent or seed) of the Poisson process. The number of points in each cloud is a Poisson random variable, each point being placed in relation to the seed independently of the other points according to a specified probability distribution. This process enables us to model the fact that fractures often occur in swarms. In this case, the semivariogram of $N(B_{\tau})$ still shows a pure nugget, but the variance of $N(B_{\tau})$ is greater than its mean.

The regionalized parent-daughter process

This is a parent-daughter process generated by parents from a regionalized Poisson process. For this process, the semivariogram of $N(B_{\tau})$ has a structure, and locally the variance of $N(B_{\tau})$ is greater than its mean.

Choice of a point process

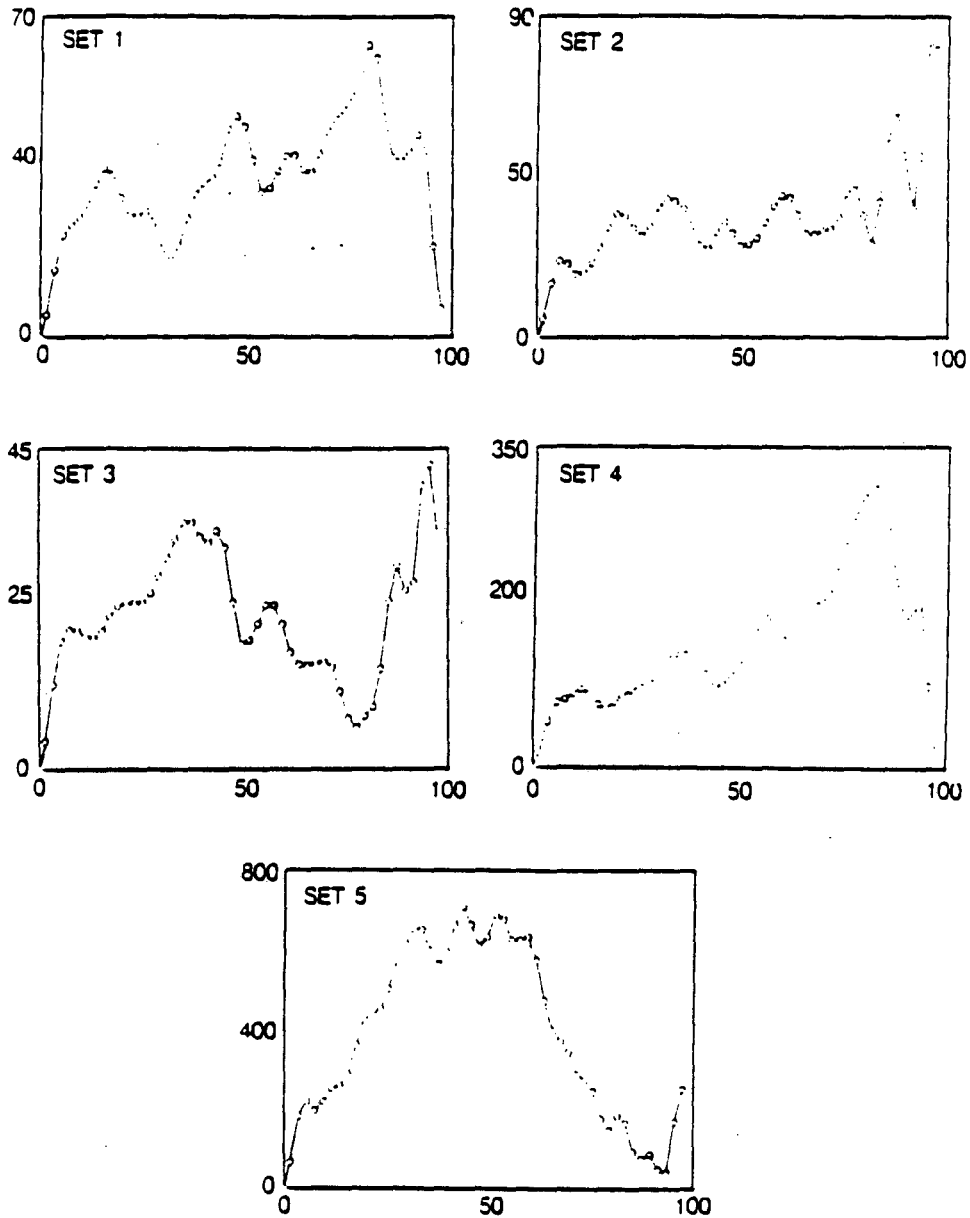
The choice of the point process for our model is based on the trace density semivariograms derived from the data. Figure 4 shows the trace density semivariograms from S1. In all cases we take the support, B , to be a 2-m \times 5-m rectangle.

The experimental semivariograms of N show two different behaviors, depending on the set. One is a true nugget effect, and the other is a semivariogram with steps, which is indicative of nested structures. The step semivariograms are the most frequent, and these are incompatible with a simple Poisson point process. For all cases, the ratio of the variance of N to its mean is generally between 4 and 5. For a simple Poisson process the ratio should be one. The regionalized Poisson process could represent the fracture centers but the underlying random rate would have to fluctuate in a way that would be difficult to describe.

In a relatively simple way, the regionalized parent-daughter process can explain both the structured aspect of all of the semivariograms for N , and the high ratio of the variance of N to its mean. The nested aspect of the semivariograms will then be due to the presence of the clouds (or swarms) of fractures, the shorter range in the semivariogram being related to the size of these clouds, and the longer range being indicative of the structure of the parents. This model was chosen.

Parameter Inference: Fitting the Model

As mentioned in the introduction, the biggest problem in fitting the model to the data is using two-dimensional information to draw inferences about three-dimensional quantities. Statistical tools developed for this purpose are described in this section.



XBL 876-2598A

Figure 4. Trace density semivariograms for five sets in S1.

The modeling is done set by set so we will have each of the parameter values for each set in S1 and S2. The quantities we need to find are

- Parameters that describe the stochastic process of fracture orientation.
- Average and standard deviation of the lognormal diameter distribution.
- Parameters that describe the parent-daughter process of fracture locations in space.

When we have specified all of these quantities we have determined a parameter solution and fitted the model to the data. In this section we discuss the determination of each of these model parameters. We begin by describing the censoring of data from small traces to compensate for measuring biases.

Censoring of small trace length data

We wish to compare our simulation of the S1 section of the drift with the S2 section. Accordingly, we want to eliminate any differences in the way data were recorded in the sections. Recall Figure 3 is a plot of all the fracture traces recorded in S1 and S2. The traces in these two cases look similar. However, one difference between S1 and S2 is a higher fraction of smaller fractures appearing in S2. Because these data were collected by several groups of workers we suspect that this difference is the result of biases in the recording of data from small traces. Also, because fractures occur down to microscopic scales one must define a cutoff length below which no fracture traces are considered. When we censor all data from traces with lengths below 0.3 m from each of S1 and S2 we find similar histograms for the remaining trace lengths. Hence, this censoring seems to equalize these measurement biases. We therefore use only these censored data realizing that we have an underestimation of the density of traces in our sampling plane. After censoring there is a total of 1008 fractures for all 5 sets in S1 and 769 fractures for all 5 sets in S2.

Parameters for orientation distribution

We model the orientation as a random field in three-dimensional space. Specifically, the idea is to find an average orientation for each set and model the deviation from the average as a random field with spatial structure.

To carry out the orientation modeling and simulation one must first characterize the mean orientation of a fracture set. The mean orientation for a particular set is taken to be the unit vector parallel to the sum of the poles in that set. There is some difficulty with this definition because of the ambiguity in the definition of a pole: if \bar{x} is a pole for a particular fracture so is $-\bar{x}$. So we must calculate the average in a slightly different way. A meaningful average is obtained in three steps:

1. Choose a trial reference vector.
2. Define the pole of a fracture to be the unit vector orthogonal to the fracture which has an angle less than 90° with the reference vector. The reference vector is kept if the maximum angle between any two poles defined this way is less than some cutoff, for example, 90° . If the maximum is greater than the cutoff, we try another reference vector.
3. Once we have found a reference vector and used it to define the poles we

sum those poles and normalize the sum. This is the pole of the mean orientation.

To continue the modeling and simulation of orientation we next have to describe the deviations of the poles in a fracture set from the mean orientation of that set. To do this the mean orientation \bar{p} (Tables 1a and 1b) is calculated for each set and the frame of reference is rotated so that \bar{p} is on the z axis. The rotation matrix we use appears in Mardia (1972) and corresponds to a rotation first about the y-axis then about the z-axis. A scatter plot of the x and y coordinates of the rotated poles represents the distribution of the orientations about the mean. This is shown for the S1 data in Figure 5.

Finally, to simulate the orientation, we simulate values of x and y. A brief description of the procedure for geostatistical simulation is given in the Appendix. As described in the Appendix, the first step in simulation is to transform x and y into Gaussian variables. Such a transformation is called anamorphosis. After anamorphosis, x and y are essentially uncorrelated as shown in Tables 2a and 2b. Hence, for purposes of simulation x and y can be taken to be independent.

The next step in the simulation of x and y is the characterization of their semi-variograms. Example semivariograms are shown for S1 in Figure 6. One can see that the nugget effect in all of them is fairly large. Some of this nugget effect is due to measurement errors, which were evaluated by Massoud and Chilès (1985). The rest of the nugget is simulated by a white noise. The structured part is simulated on a regular grid following techniques outlined in the Appendix. The relevant parameters for S1 and S2 are given in Tables 1a and 1b. The structured parts of x and y for a given fracture are then found by choosing the values at the simulated grid point closest to the fracture center.

Finally, the orientation of a given fracture is taken as the mean for the set plus a component of white noise plus the structured component from the geostatistical simulation.

Determination of the disc diameter distribution

The trace length data are used to find the diameter distribution. As we have mentioned before the determination of the diameter distribution from trace lengths is an ill-posed problem. One reason for this is that the sampling area is finite so that many traces are truncated by the boundaries of this area. Hence, information about the upper tails of the trace length distribution and diameter distribution is not available. A second reason is that the process of finding the diameter distribution from the trace length distribution is sensitive to any biases or noise in the data. This has the effect that a small change in the trace length distribution causes a large change in the resulting diameter distribution.

A functional relationship between the distribution of fracture trace lengths and the distribution of fracture diameters not accounting for truncation effects was developed by Warburton (1980), and is given by

$$f(l) = 1/\bar{D} \int_0^{\infty} \frac{g(D)}{\sqrt{D^2 - l^2}} dD.$$

Table 1a. Mean orientations and parameters of reduced orientation variograms for S1.

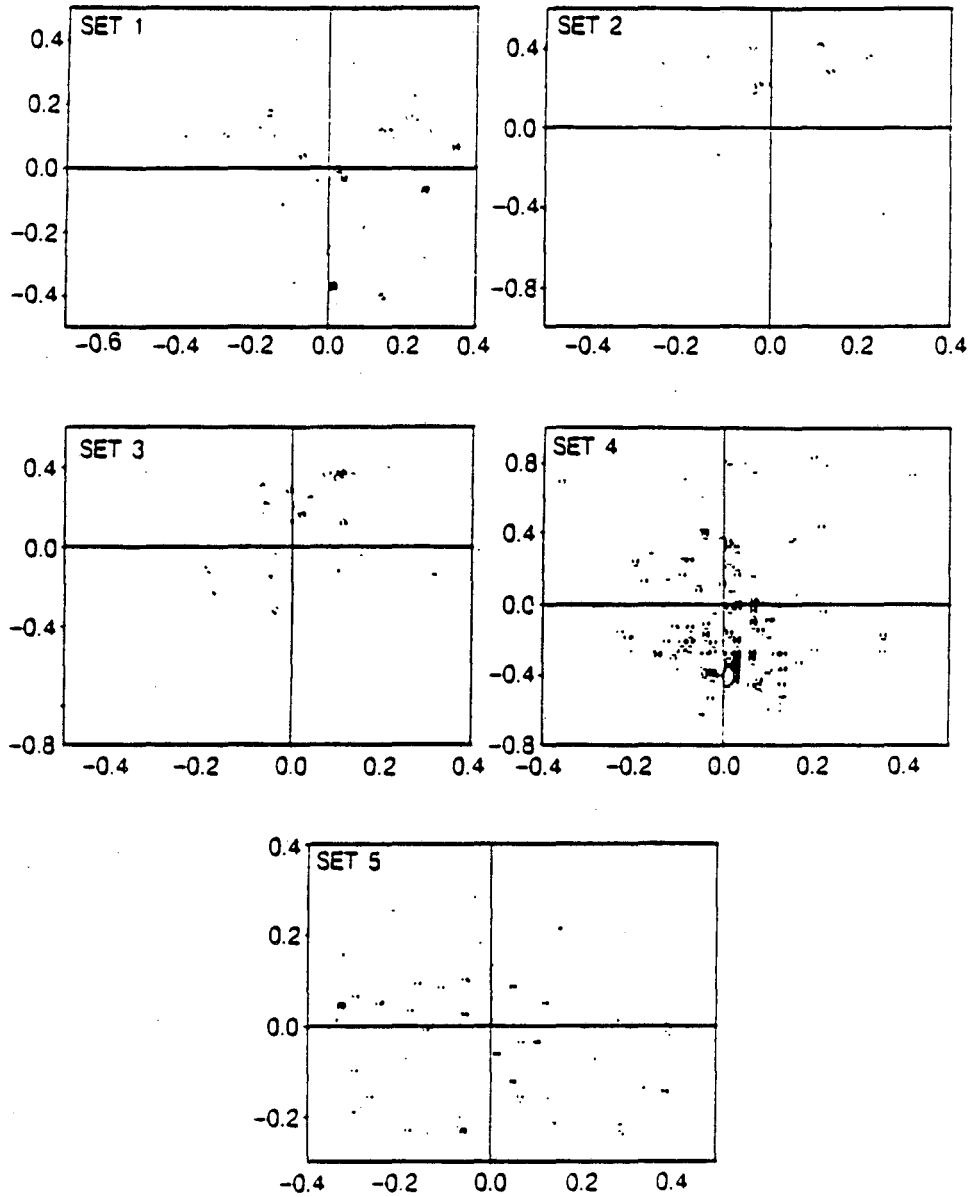
Set	Mean orientation		x variogram**			y variogram**		
	θ°	ϕ°	nugget	sill	range m	nugget	sill	range m
1	289	9.6	1.0	1.5	40	0.75	1.3	10
2	274	44.2	1.0	1.25	40	1.0	1.0	-
3	79	46.2	1.0	1.0	-	1.0	1.0	-
4	351	87.1	0.75	1.12	50	0.75	1.5	50
5	263	88.0	0.8	1.0	50	0.8	1.25	40

**These are standard spherical coordinates with positive x-axis pointing north and positive y-axis pointing west.

Table 1b. Mean orientations and parameters of reduced orientation variograms for S2.

Set	Mean orientation		x variogram**			y variogram**		
	θ°	ϕ°	nugget	sill	range m	nugget	sill	range m
1	231	4.5	.75	1.2	13	1.0	1.0	-
2	250	45.7	.75	1.25	40	0.9	1.4	18
3	66	44.9	1.0	1.9	50	0.9	0.9	-
4	1	88.8	0.95	1.20	30	1.10	1.10	-
5	276	81.8	0.8	0.8	-	1.10	1.50	50

**These are standard spherical coordinates with positive x-axis pointing north and positive y-axis pointing west.



XBL 876-2601A

Figure 5. Scatter plot of rotated orientations before anamorphosis for five sets in S1.

Table 2a. Correlation coefficients for x and y components of the orientation data after anamorphosis, S1.

Set	Correlation coefficient
1	-0.136
2	0.092
3	0.283
4	-0.141
5	-0.128

Table 2b. Correlation coefficients for x and y components of the orientation data after anamorphosis, S2.

Set	Correlation coefficient
1	0.194
2	-0.068
3	-0.126
4	0.196
5	-0.038

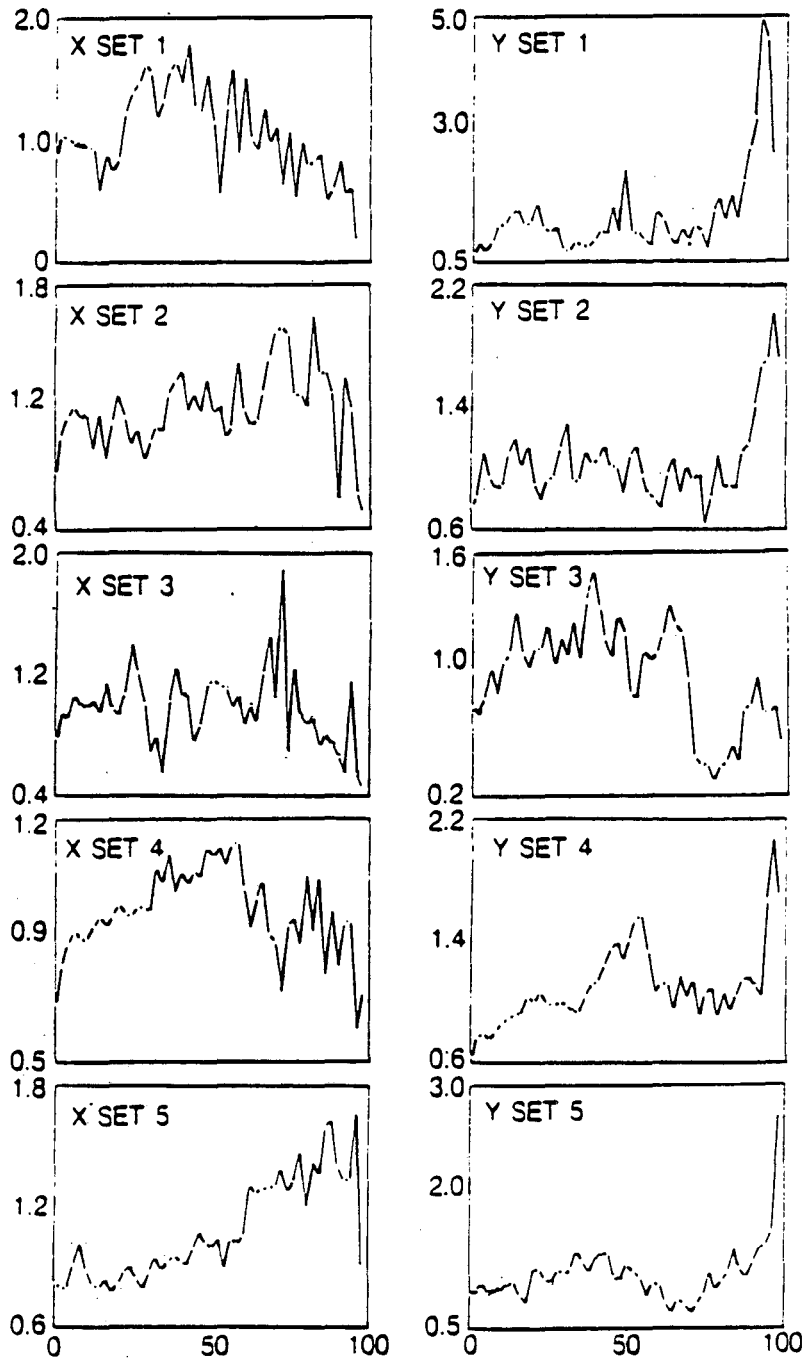
where

D = diameter of a given fracture.

g(D) = pdf (probability density function) of fracture diameters.

f(l) = pdf of fracture traces.

$$\bar{D} = \text{mean of } D = \int_0^{\infty} D g(D) dD.$$



XBL 876-2600A

Figure 6. Semivariograms of orientation after anamorphosis for five sets in S1.

So, given a particular probability density function for fracture diameters, $g(D)$, we can evaluate the integral to obtain the density of trace lengths $f(l)$. One can then compare the computed density of trace lengths to that obtained from the field data. By trial and error, one can find a reasonable, but not necessarily unique distribution for fracture diameters. This process ignores truncation effects.

To include the effects of truncation, we use a Monte Carlo procedure that simulates traces in the drift. First, we assume a lognormal distribution for fracture diameters with a given standard deviation and mean. Next a number of discs with this diameter distribution are placed in space with orientations chosen at random from measured orientations in the drift. We calculate the intersections of these fractures with a rectangle representing the drift wall. The resulting traces are analyzed to get a trace length distribution including truncation percentages and separate distributions for traces where one or two endpoints appear. These distributions are compared to those from the data. This process is repeated for a range of values of mean and standard deviation of diameters until a good match is found between actual trace lengths and simulated trace lengths.

Calculation of the trace density semivariogram from the data

To complete the model fitting we need to find the parameters of the parent-daughter point process which describes the location of fracture centers. We have said that these parameters are found by matching plane density semivariograms. Figure 4 shows the trace density semivariograms calculated from the S1 data. A similar computation was done for S2. We describe how these semivariograms were calculated.

The drift mappings are in rectangles measuring $100 \text{ m} \times 2 \text{ m}$ and $80 \text{ m} \times 2 \text{ m}$ respectively (Figure 3). Length is in the x direction and width in the y direction. Hence, $0 \text{ m} \leq x \leq 100 \text{ m}$ or 80 m and $0 \text{ m} \leq y \leq 2 \text{ m}$. To calculate the experimental trace density semivariogram we count the number of traces in a window that measures $5 \text{ m} \times 2 \text{ m}$ and is centered at the point \bar{x} , then multiply this number by an "orientation correction factor" that adjusts for the fact that the fractures are not perpendicular to the sampling plane. Let $E_{\bar{x}}$ denote the resulting number of traces adjusted for orientation in the window centered at \bar{x} . We slide the window centered on $\bar{x} = (x,y)$, across the length of the drift, fixing $y = 1$ and letting x range from 2.5 m to 97.5 m (or 77.5 m for S2) using increments of size 1 m . $\gamma(h)$ is estimated via

$$\gamma(h) = \frac{1}{2} \frac{1}{n_h} \left\{ \sum_{\{(\bar{x}, \bar{w}) : |\bar{x} - \bar{w}| = h\}} (E_{\bar{x}} - E_{\bar{w}})^2 \right\}$$

where n_h is the number of window pairs with centers that are a distance h apart. Typically, experimental semivariograms have small sampling variations for h less than half the drift length.

To describe the orientation correction factor, let θ be the angle between a fracture pole and the sampling plane measured in degrees. We always take $0^\circ \leq \theta < 90^\circ$. If a fracture with angle θ is placed randomly in space the probability that the fracture

intersects the sampling plane is proportional to $\cos\theta$. Hestir et al. (1987) use this result to show that the orientation correction factor for a particular window is

$$\frac{1}{\overline{\cos(\theta)}}$$

where $\overline{\cos(\theta)}$ is the average of the $\cos(\theta)$'s for all fractures in the window.

Theoretical trace density semivariogram for the parent-daughter model

We now describe how to find the parameters for the parent-daughter model. These parameters define the distributions of the density of parents and of the number of daughters per parent, and the dispersion of the daughters around the parents. In the Appendix, we derive the theoretical two-dimensional trace density semivariogram results from a given parameterization of the three-dimensional parent-daughter model. This enables us to establish the relationship between the parameters of the parent-daughter model and the experimental semivariogram. These formulas were originally worked out in Deverly (1986) for a model of nugget deposits. In our derivation for discs, the trace density semivariogram is calculated by conditioning on a fixed realization of parents (i.e., assume there is a fixed realization of parents) and then removing the conditioning. The end results along with some notation are shown below.

Let x be a point in three-dimensional space, R^3 and $\Lambda_p(x)$ be the stationary random process for the parent rate. We assume that Λ_p is a Gaussian process with covariance structure defined by a spherical semivariogram with a given range and sill. Also let

- $\bar{\lambda}_p = E(\Lambda_p(x))$, the average of Λ_p .
- $C_{\Lambda_p}(h) = E(\Lambda_p(x+h)\Lambda_p(x))$, this is the non-centered covariance of Λ_p .
- $\lambda_D =$ rate of daughters, i.e., the number of daughters is taken to be Poisson with rate λ_D .
- $F(x) =$ probability distribution function for the location of a daughter relative to the parent. In our model we always assume the displacements $(x,y,z) = x$, are independent, identically distributed, mean 0, Gaussian random variables.
- B, \hat{B} be windows in the sampling plane.
- $Q(B) =$ the number of traces in B .
- $\Psi(B,x) =$ probability that a daughter from a parent at x intersects B .

The parameters that specify the model are

- The average, range, and sill of the parent rate Λ_p ,
- The rate, λ_D , of the Poisson number of daughters around each parent, and
- The standard deviation of the Gaussian dispersion of daughters about the parents.

In terms of these parameters we find, as shown in the Appendix:

$$E(Q(B)) = \bar{\lambda}_p \lambda_D \int_{R^3} \Psi(B,x) dx = \bar{\lambda}_p \lambda_D \text{area}(B) \bar{D} \quad (1)$$

and

$$\begin{aligned}
 E(Q(B)Q(\hat{B})) &= \lambda_D^2 \int_{R^j} \int_{R^j} \Psi(B,x) \Psi(\hat{B},y) C_{\Lambda_p}(x-y) dx dy & (2) \\
 &+ \bar{\Lambda}_p \lambda_D^2 \int_{R^j} \Psi(B,x) \Psi(\hat{B},x) dx \\
 &+ \bar{\Lambda}_p \lambda_D \int_{R^j} \Psi(B \cap \hat{B}, x) dx .
 \end{aligned}$$

Numerical modeling: Generation of the fracture mesh

Once the parameter solution is available, the following steps are taken to create a realization of the fracture system.

1. A simulation of Λ_p is made in a three-dimensional region. We assume that Λ_p is a Gaussian random field with average large enough in comparison to its standard deviation so that negative values for rate occur with low probability. Negative values are set at zero. The covariance structure is specified by a spherical semivariogram having a range and sill given in the parameter solution.
2. Parents are simulated on small subregions, ΔV_x , centered at points x , with constant volume Δx . To simulate the parents in ΔV_x , we first find the value of $\Lambda_p(x)$ (if $\Lambda_p(x) < 0$ we set $\Lambda_p(x) = 0$).
3. Next, we pick the number of parents in ΔV_x according to a Poisson process of rate $\Lambda_p(x)\Delta x$.
4. Each parent in ΔV_x is placed at random in ΔV_x according to a uniform distribution.
5. For each parent we pick a number of daughters according to a Poisson distribution with rate λ_D .
6. Next, the random locations of fractures (daughters) are determined. This is done by choosing displacements from the parent in the x , y , and z directions independently according to a Gaussian distribution with mean 0 and variance specified by the parameter solution.
7. The orientation is determined in three steps. Start with the mean for the set. Add the structured part from the orientation simulation described above. Finally, add a random component as determined by the nugget of the orientation semivariogram.
8. The fracture diameter is chosen from its global distribution.

To check the simulations, we can take a sample of generated fractures and calculate the sample average for diameter and orientation to make sure they fall within reasonable limits. We can also record the number of fractures generated in the generation volume V , and check to see that this falls in a reasonable range. To do this note that

$$E(F(V)) = \bar{\lambda}_p \lambda_D \text{volume}(V)$$

and

$$\begin{aligned} \text{Var}(F(V)) = & \bar{\lambda}_p \lambda_D \text{volume}(V) + \lambda_D^2 \bar{\lambda}_p \int_{R^j} \Psi^2(V,x) dx \\ & + \lambda_D^2 \int_{R^j} \int_{R^j} [C_{\lambda_p}(x-y) - \bar{\lambda}_p^2] \Psi(V,x) \Psi(V,y) dx dy . \end{aligned}$$

where $F(V)$ denotes the number of fractures occurring in volume V . Equations (1) and (2) can be used to verify these expressions with $\Psi(V,x)$ replacing $\Psi(B,x)$.

Connectivity Study

We can also make a study of the connectivity in our mesh simulations. Observations at Fanay show that the section of the drift called S1 is wet and the section labeled S2 is dry. We expect that our connectivity studies will reflect this difference.

A measure of connectivity is defined as follows. The first step is to place an artificial fracture somewhere in the center of our simulation: this is our starting point which we call the level 0 fracture. Level 1 fractures are defined to be all fractures that intersect the level 0 fracture. In general, level k fractures are defined to be all fractures that intersect a level $k-1$ fracture and have not been previously assigned to a level. The recorded number of fractures in each level is our measure of connectivity. We call these the level sizes.

One way to view this measure of connectivity is as a simple summary of the number of paths through which water can flow if injected into the level 0 fracture. Some work needs to be done to examine growth and the variability of the level sizes in the simulations.

A practical limitation of this idea is that the number of fractures that can be examined to find level sizes is limited by computing facilities. Also, of course, this is a method that is suited to examination of simulations and not to "real life" fracture meshes. Its relevance is therefore dependent on the relevance of the simulation.

Conclusion

We have described some techniques for the simulation of a fracture network based on data from a real fracture system. The simulation reproduces the spatial variability of fracture density and orientation. To accomplish this, we have developed a stochastic model that incorporates this spatial variation. We have also described how the model can be fit to the data and have introduced a measure of connectivity for fracture mesh simulations.

Acknowledgment

This work is the product of cooperation between Lawrence Berkeley Laboratory (LBL) and the French Bureau de Recherches Géologiques et Minières (BRGM). Support was provided to LBL by the U.S. Department of Energy under Contract No. DE-AC03-76SF00098 and to BRGM by the Agence Française pour les Economies d'Energie. The data used here were taken in the Fanay-Augères mine owned by Cogema under contract with the French Commissariat à l'Energie Atomique. The authors are indebted to Paul Witherspoon of LBL and Bernard Feuga of BRGM.

Literature Cited

1. Alfaro, M., 1980. "The Random Coin Method: Solution to the Problem of Simulation of a Random Function in the Plane." *Mathematical Geology*, 12.
2. Barbreau, A., B. Come, S. Derlich, E. Durand, G. de Marsily, P. Peaudecerf, and G. Vouille, 1985. "Experiments Performed on Granite in the Underground Research Laboratory at Fanay-Augères, France." *Proc. Internat. Symp. on Coupled Processes Affecting the Performance of a Nuclear Waste Repository*, Lawrence Berkeley Laboratory, Berkeley, CA, Sept.
3. Cacas, M. C., E. Ledoux, G. de Marsily, and B. Tillie, 1987. *Etude de l'Effet d'Echelle en Milieu Fissuré*. Report of Ecole Nationale Supérieure des Mines de Paris.
4. Dershowitz, W., 1984. "Rock Joint Systems." Ph.D. dissertation, Massachusetts Institute of Technology, Cambridge, MA.
5. Deverly, F., 1984. "Echantillonnage et Géostatistique." thèse, Ecole Nationale Supérieure des Mines de Paris.
6. Gros, Y., 1982. *Etude Structurale de la Mine de Fanay-Augères—Géométrie, Cinématique et Chronologie des Fractures*, BRGM report.
7. Hestir, K., Jean-Paul Chiès, Jane Long, and Daniel Billaux, 1987. "Three Dimensional Modeling of Fractures in Rock: From Data to a Regionalized Parent Daughter Model." *AGU Monograph on Flow in Unsaturated Rock*.
8. Journel, A. G. and Ch. J. Huijbregts, 1978. *Mining Geostatistics*, Academic Press Inc., London.
9. Lassagne, D., 1983. *Essai de Caractérisation du Milieu Fracturé en Massif Granitique*, BRGM report 83 SGN 576 GEC, 45060 Orléans, France.
10. Long, J.C.S. and D. M. Billaux, 1987. "From Field Data to Fracture Network Modeling—An Example Incorporating Spatial Structure." *Water Resources Research*, 23(7) pp. 1201-1216.
11. Long, J.C.S. and P. A. Witherspoon, 1985. "The Relationship of Degree of Interconnection to Permeability in Fracture Networks." *Journal of Geophysical Research*, 90(B4), pp. 3087-3098.
12. Long J.C.S., J. S. Remer, C. R. Wilson, and P. A. Witherspoon, 1982. "Porous Media Equivalents for Networks of Discontinuous Fractures." *Water Resources Research*, 18(3), pp. 645-658.
13. Mardia, K. V., 1972. *Statistics of Directional Data*, Academic Press Inc., London.
14. Massoud, H. and J. P. Chiès, 1985. *Approche Stochastique de l'Erreur Liée à la Position et à l'Orientation d'une Fracture*, BRGM technical note.
15. O'Sullivan, F., 1986. A Statistical Perspective on Ill-posed Inverse Problems. *Statistical Science*, Vol. 1, No. 4, pp. 502-527.
16. Ripley, B. D., 1981. *Spatial Statistics*, John Wiley and Sons, New York.

17. Robinson, P., 1984. "Connectivity, Flow and Transport in Network Models of Fracture Media." Ph.D. dissertation, St. Catherine's College, Oxford.
18. Rouleau, A., 1984. "Statistical Characterization and Numerical Simulation." Ph.D. dissertation, Univ. of Waterloo, Waterloo, Ontario.
19. Stoyan, D., W. S. Kendall, and J. Mecke, 1987. *Stochastic Geometry and Its Applications*, John Wiley and Sons, New York.
20. Warburton, P. A., 1980. "A Stereological Interpretation of Joint Trace Data." *Int. Jour. Rock Mech. Min. Sci. and Geomech. Abstr.*, Vol. 17, pp. 181-190, Pergamon Press Ltd., Oxford.

APPENDIX

Geostatistical Simulation Procedure

To describe the process of geostatistical simulation we first define a few terms. Let $X(\vec{r})$ be a random field in n -dimensional space, $n = 1, 2, 3$. We have $\gamma(\vec{h}) = 1/2 E(X(\vec{r} + \vec{h}) - X(\vec{r}))^2$. It is assumed that $\gamma(\vec{h}) = \gamma(|\vec{h}|) = \gamma(h)$, where $h = |\vec{h}|$, that is, γ is isotropic. Generalizations to anisotropic γ can be made but are not discussed here.

Now assume X is observed at points $\vec{r}_1, \vec{r}_2, \dots, \vec{r}_n$. We can estimate $\gamma(h)$ with

$$\gamma(h) = \frac{1}{2} \frac{1}{n_h} \left\{ \sum_{(\vec{r}_i, \vec{r}_j : |\vec{r}_i - \vec{r}_j| = h)} (X(\vec{r}_i) - X(\vec{r}_j))^2 \right\}$$

where n_h is the number of points $\vec{r}_1, \vec{r}_2, \dots, \vec{r}_n$ that are distance h apart (within a certain tolerance). Also, we can see if X is a Gaussian process by examining the histogram of the observed values $X(\vec{r}_1), X(\vec{r}_2), \dots, X(\vec{r}_n)$.

If X is a Gaussian process with semivariogram γ , then the simulation of X is a straightforward procedure using either the turning bands method (Journel and Huijbregts, 1978) or the random spheres method (Alfaro, 1980). We use the random sphere method in our work.

If X is not a Gaussian process we first transform it into one. This is done by using a transformation f , called an anamorphosis (or graphical transformation). Specifically, f is a one to one function constructed so that the histogram of $f(X(\vec{r}_1)), f(X(\vec{r}_2)), \dots, f(X(\vec{r}_n))$ has a Gaussian shape. It is then assumed that $f(X)$ is a Gaussian process. Details of the construction of f can be found in Journel and Huijbregts (1978, pp. 478).

Once the anamorphosis f is found the next step is to simulate the transformed process $f(X)$. This is done as described above by estimating the semivariogram of $f(X)$ using

$f(X(\bar{t}_1)), f(X(\bar{t}_2)), \dots, f(X(\bar{t}_n))$ and employing the random spheres method. Finally, the resulting simulation of $f(X)$ is transformed by f^{-1} yielding the simulation of X .

Calculation of the Theoretical Trace Density Semivariogram for the Parent-daughter Model

Below we use notation given in the section on parameter inference. Divide space into small disjoint sets ΔV_k centered at x_k with volume Δx_k . Let P_k denote the number of parents occurring in ΔV_k . Let $Q_k(B)$ denote the number of daughters appearing in B from parents occurring in ΔV_k . To condition on Λ_p we suppose Λ_p is a fixed function on R^3 , $\Lambda_p : R^3 \rightarrow R^+$, (R^+ = the set of non-negative real numbers). E_{Λ_p} will denote expectation given a fixed Λ_p . Also note that when Λ_p is fixed, P_k is a Poisson random variable with rate $\Lambda_p(x_k)\Delta x_k$.

We do a second conditioning by assuming that P_k is fixed for each k , in other words, the ensemble of parent points is fixed. $E_{\Lambda_p, \Omega}$ will denote expectation given a fixed Λ_p and fixed ensemble, Ω . Now, for fixed Λ_p and Ω the following statements hold:

- 1) $Q_k(B)$ is a Poisson random variable with rate $P_k \lambda_D \Psi(B, x_k)$, hence $E_{\Lambda_p, \Omega}(Q_k(B)) = P_k \lambda_D \Psi(B, x_k)$.
- 2) For $k \neq j$, $Q_k(B)$ and $Q_j(B)$ are independent.
- 3) $Q_k(B_1)$ and $Q_j(B_2)$ are independent for any k and j when B_1 and B_2 are disjoint.
- 4) $E_{\Lambda_p}(X) = E_{\Lambda_p}(E_{\Lambda_p, \Omega}(X))$ and $E(X) = E(E_{\Lambda_p}(X))$.

Finally, notice that

$$Q(B) = \sum_k Q_k(B)$$

$$Q(\hat{B}) = \sum_k Q_k(\hat{B})$$

and

$$Q(B)Q(\hat{B}) = \sum_{k \neq j} Q_k(B)Q_j(\hat{B}) + \sum_k Q_k(B)Q_k(\hat{B}) .$$

Now, conditioning on Λ_p and Ω yields

$$E_{\Lambda_p, \Omega}(Q(B)) = \sum_k P_k \lambda_D \Psi(B, x_k) .$$

For calculation of $E_{\Lambda_p, \Omega}(Q(B)Q(\hat{B}))$ first recall the fact that if N_1, N_2 and N_3 are independent Poisson random variables with rates $\lambda_1, \lambda_2,$ and λ_3 then

$$E((N_1 + N_2)(N_2 + N_3)) = (\lambda_1 + \lambda_2)(\lambda_2 + \lambda_3) + \lambda_2 .$$

This implies that

$$E_{\Lambda_p, \Omega}(Q_k(B)Q_k(\hat{B})) = P_k^2 \lambda_D^2 \Psi(B, x_k) \Psi(\hat{B}, x_k) + P_k \lambda_D \Psi(B \cap \hat{B}, x_k)$$

which gives

$$\begin{aligned} E_{\Lambda_p, \Omega}(Q(B)Q(\hat{B})) &= E_{\Lambda_p, \Omega}(\sum_{i \neq j} Q_i(B)Q_j(\hat{B})) + E_{\Lambda_p, \Omega}(\sum_k Q_k(B)Q_k(\hat{B})) \\ &= \sum_{i \neq j} \lambda_D^2 P_i P_j \Psi(B, x_i) \Psi(B, x_j) \\ &\quad + \sum_k P_k^2 \lambda_D^2 \Psi(B, x_k) \Psi(\hat{B}, x_k) + \sum_k P_k \lambda_D \Psi(B \cap \hat{B}, x_k) . \end{aligned}$$

Next we remove the conditioning on the ensemble Ω .

$$E_{\Lambda_p}(Q(B)) = E_{\Lambda_p}(E_{\Lambda_p, \Omega}(Q(B))) = \sum_k \Lambda_p(x_k) \Delta x_k \lambda_D \Psi(B, x_k)$$

and

$$\begin{aligned} E_{\Lambda_p}(Q(B)Q(\hat{B})) &= E_{\Lambda_p}(E_{\Lambda_p, \Omega}(Q(B)Q(\hat{B}))) \\ &= \sum_{i \neq j} \lambda_D^2 \Lambda_p(x_i) \Lambda_p(x_j) \Psi(B, x_i) \Psi(B, x_j) \Delta x_i \Delta x_j \\ &\quad + \sum_k ((\Lambda_p(x_k) \Delta x_k)^2 + \Lambda_p(x_k) \Delta x_k) \lambda_D^2 \Psi(B, x_k) \Psi(\hat{B}, x_k) \\ &\quad + \sum_k \Lambda_p(x_k) \Delta x_k \lambda_D \Psi(B \cap \hat{B}, x_k) . \end{aligned}$$

Lastly, we remove the conditioning on Λ_p .

$$E(Q(B)) = E(E_{\Lambda_p}(Q(B))) = \sum_k \bar{\Lambda}_p \Delta x_k \lambda_D \Psi(B, x_k)$$

and

$$\begin{aligned}
 E(Q(B)Q(\hat{B})) &= E(E_{\Lambda_p}(Q(B)Q(\hat{B}))) = \\
 &= \sum_{k \neq j} \lambda_0^2 \Psi(B, x_k) \Psi(\hat{B}, x_j) C_{\Lambda_p}(x_j - x_k) \Delta x_k \Delta x_j \\
 &+ \sum_k \lambda_0 \bar{\Lambda}_p \Psi(B, x_k) \Psi(\hat{B}, x_k) \\
 &+ \sum_k (\Delta x_k)^2 (\text{bounded term}) \\
 &+ \sum_k \bar{\Lambda}_p \Delta x_k \lambda_0 \Psi(B \cap \hat{B}, x_k) .
 \end{aligned}$$

Now, letting $\Delta x_k \rightarrow 0$ gives the result

$$E(Q(B)) = \bar{\Lambda}_p \lambda_0 \int_{R^3} \Psi(B, x) dx = \bar{\Lambda}_p \lambda_0 \text{area}(B) \bar{D} \quad (1)$$

and

$$\begin{aligned}
 E(Q(B)Q(\hat{B})) &= \lambda_0^2 \int_{R^3} \int_{R^3} \Psi(B, x) \Psi(\hat{B}, y) C_{\Lambda_p}(x - y) dx dy \\
 &+ \bar{\Lambda}_p \lambda_0^2 \int_{R^3} \Psi(B, x) \Psi(\hat{B}, x) dx \\
 &+ \bar{\Lambda}_p \lambda_0 \int_{R^3} \Psi(B \cap \hat{B}, x) dx .
 \end{aligned} \quad (2)$$

Interdistance Statistic

Using conditioning methods as those employed above one can derive some interdistance statistics. One result in this direction shows that for S equal to the sum of interdistances between all possible pairs of trace centers in a particular window

$$E(S) = \frac{1}{2} \bar{\Lambda}_p \lambda_0^2 \int_{R^3} \Psi^2(B, x) h(x) dx + \frac{1}{2} \lambda_0^2 \int_{R^3} \int_{R^3} C(x - \xi) H(x, \xi) \Psi(B, x) \Psi(B, \xi) dx d\xi .$$

where

$$x = (x, y, z)$$

$$\xi = (\xi, \eta, \zeta) .$$

the sampling window is defined in the x -direction by $a < x < b$, $\sigma =$ standard deviation of the

*LAWRENCE BERKELEY LABORATORY
TECHNICAL INFORMATION DEPARTMENT
UNIVERSITY OF CALIFORNIA
BERKELEY, CALIFORNIA 94720*